Optimizing the proximity effect along the BCS side of the BCS-BEC crossover

V. Piselli,[1] S. Simonucci,[1,2] and G. Calvanese Strinati[1,2,3,*]

[1]*School of Science and Technology, Physics Division, Università di Camerino, 62032 Camerino (MC), Italy*

[2]*INFN, Sezione di Perugia, 06123 Perugia (PG), Italy*

[3]*CNR-INO, Istituto Nazionale di Ottica, Sede di Firenze, 50125 Firenze (FI), Italy*

(Received 31 July 2018; revised manuscript received 21 September 2018; published 11 October 2018)

The proximity effect, which arises at the interface between two fermionic superfluids with different critical temperatures, is examined with a nonlocal (integral) equation whose kernel contains information about the size of Cooper pairs that leak across the interface. This integral approach avoids reference to the boundary conditions at the interface that would be required with a differential approach. The temperature dependence of the pair penetration depth on the normal side of the interface is determined over a wide temperature range also varying the interparticle coupling along the BCS side of the BCS-BEC crossover independently on both sides of the interface. In this way, the size of Cooper pairs evolves from being much larger than (BCS limit) the interparticle distance to being comparable with (unitarity limit, halfway between the BCS and BEC limits) the interparticle distance. Conditions are then found for which the proximity effect is optimized in terms of the extension of the pair penetration depth.

DOI: 10.1103/PhysRevB.98.144508

I. INTRODUCTION

Recently, a novel approach for designing and tailoring entirely new classes of materials through "proximity effects" has been suggested, which could overcome limitations inherent to more conventional (such as doping) methods [1]. Quite generally, proximity effects can rely on superconducting, magnetic, or topological properties. Here, we consider theoretically the proximity effect that arises across the interface between two superconductors with different critical temperatures. In this situation, the paired state in the superconductor at the left (L) of the interface, keeping a temperature T below its critical temperature T_c^L, leaks into the superconductor at the right (R) of the interface whose critical temperature T_c^R is instead smaller than T. The novelty is that the (left) superconductor with higher-temperature T_c^L can be made to reach the so-called unitarity limit of the BCS-BEC crossover where the size of the Cooper pairs becomes comparable with the interparticle spacing [2] in order to study the optimal conditions for the proximity effect to occur.

The above is a typical problem in inhomogeneous superconductivity, which can, in principle, be treated in terms of the Bogoliubov–de Gennes (BdG) equations with the inclusion of boundary effects [3,4]. As summarized in Ref. [5], however, most of the early knowledge about the proximity effect was gained in terms of the linearized Gor'kov equation for the gap parameter [4], which holds in the vicinity of the critical temperature. More recently, the BdG equations were used [6] to demonstrate the connection between the proximity effect and the Andreev reflection [7].

A characteristic quantity in the context of the proximity effect is the (temperature dependent) *pair penetration depth* (or thickness of the leakage region on the normal side of the interface, which we will refer to as ξ_R according to our reference geometry). This quantity was estimated theoretically in Ref. [8] in terms of the Eilenberger formalism [9] (or of its simplified Usadel version for the dirty limit [10]), which is a "quasiclassical" approximation that greatly reduces the complexity of the Gor'kov equations by averaging out the fast oscillations (on the order of the Fermi wavelength) arising in the relative coordinate of Cooper pairs. By this approach in Ref. [8] it was possible to explore a wide interval of temperature which extends away from the immediate vicinity of the critical temperature although still in the weak-coupling (BCS) regime of the superconducting coupling when a well-defined underlying Fermi surface is present.

Experiments could as well be directed at determining the temperature dependence of the pair penetration depth on the normal side also in systems where the superconducting coupling may not be so weak along the lines of the original experimental work of Ref. [11]. In that work, critical-current measurements were performed in high-T_c superconducting-normal-superconducting junctions, yielding an exponential dependence of the critical current on the thickness of the barrier which is a characteristic feature of the proximity effect. In particular, from Fig. 4 of Ref. [11] one can identify a *two-slope* dependence of the decay length in different temperature regimes (in the vicinity of T_c^R and of T_c^L), a result which is in line with that obtained theoretically in Ref. [8] (albeit in the weak-coupling regime only).

This two-slope dependence of the pair penetration depth was qualitatively put in relation in Ref. [12] with the different temperature dependences that, in the normal phase above T_c, characterize the healing length (due to *inter*pair correlations) and the pair coherence length (due to *intra*pair correlations). In Ref. [12], however, the change in slope between these two lengths could be clearly identified only over a temperature

*giancarlo.strinati@unicam.it

range on the order of the Fermi temperature T_F, whereas in the proximity effect the pair penetration depth can be determined only over a much more limited temperature range since, in practice, $T_c^L \ll T_F$. In addition, in Ref. [12] the two lengths were separately determined by two independent calculations, which could thus not identify them as the separate limiting values (close to and far away from the critical temperature T_c) of the same physical length. In Ref. [12], the study of these two lengths was systematically extended to the whole BCS-BEC crossover throughout which the system evolves with continuity from the presence of large overlapping Cooper pairs (BCS regime) to the presence of dilute composite bosons (BEC regime).

With these premises, it appears highly desirable to study theoretically the proximity effect when either one of the fermionic systems at one side of the interface (or when even both of them) spans the whole BCS side of the BCS-BEC crossover up to the highest attainable temperature in the superfluid phase. To this end, here we approach the problem in terms of a nonlocal (integral) equation for the gap parameter, which contains a kernel that depends on the gap parameter itself in a highly nonlinear way and thus extends the linearized Gor'kov equation used originally in Ref. [3] not only away from the vicinity of the critical temperature, but also along the BCS-BEC crossover. This integral equation was derived in Ref. [13] by a double coarse-graining procedure applied to the BdG equations, which deals with the magnitude and phase of the gap parameter on a different footing (for this reason, the equation was referred to as the NLPDA equation with the acronym standing for nonlocal phase density approximation). The properties and range of validity of the NLPDA equation were later discussed in Ref. [14] where an efficient practical method for finding its solution numerically was also provided. A key property, which renders the NLPDA equation ideally suited to deal with the proximity effect, is that the spatial extension of its kernel corresponds to the size of the Cooper pairs for any coupling throughout the BCS-BEC crossover.

By making use of this approach, we will determine the pair penetration depth ξ_R on the normal side of the interface over a wide temperature range and under quite different physical conditions on the two sides of the interface thereby enabling us to identify the limiting behaviors (close to T_c^R and to T_c^L) of this length in terms of a *single* calculation. In addition, by this approach we will have the flexibility of modeling the interparticle coupling and the trapping potential in a physically smooth way across the interface that separates the left and right superconductors, and we will avoid at the same time any reference to the boundary conditions at the interface [3,4]. This property could, in turn, be used to identify "effective" boundary conditions for the gap parameter and its derivative across the interface, which may then be adopted in local (differential) versions of the present approach.

The main results of our calculations are as follows:

(i) For given coupling on the left of the interface, the pair penetration depth ξ_R on the right is found to increase (thereby amplifying the relevance of the proximity effect) when the bulk values Δ_L and Δ_R, reached by the gap profile deep on the left and right of the interface, respectively, differ appreciably from each other. This finding could also be used in reverse in cases one would instead like to attenuate the occurrence of the proximity effect.

(ii) When the coupling on the left of the interface is increased toward the unitary limit such that the Cooper pair size decreases and becomes comparable with the interparticle distance, the pair penetration depth ξ_R on the right is found to decrease too. At the same time, however, there is an increase in the range of temperatures over which the proximity effect can occur. Optimizing the proximity effect may thus require one to compromise between these two contrasting behaviors.

(iii) The temperature dependence of ξ_R turns out to reproduce the behaviors in the vicinity of both T_c^R and T_c^L that were anticipated in Ref. [8] (although in that reference for the extreme weak-coupling limit only). Our calculations extend these findings over a much wider coupling range along the BCS side of the BCS-BEC crossover.

(iv) The pair penetration depth ξ_R turns out to be essentially independent from the shape of the barrier, a feature which can be readily varied within the present approach.

(v) A "negative" proximity effect also occurs for the left superconductor with the higher-temperature T_c^L, resulting in a marked depression of the gap profile which can extend far away from the interface.

In contrast to the present approach, more conventional treatments of the proximity effect in terms of the BdG equations [15] have largely focused on the region close to the interface (thereby not extracting the behavior of ξ_R), have described the interfacial scattering by a simple δ-function potential, have not pushed the calculation to the vicinity of the bulk transition temperature in the superconducting region, and, most importantly, have been limited only to the BCS (weak-coupling) limit of the BCS-BEC crossover. However, consideration of the BCS-BEC crossover appears important not only for ultracold Fermi gases and nuclear systems [2], but also for recently acquired growing attention in condensed matter where experimental signatures of preformed Cooper pairing have been reported for Fe-based superconductors [16]. In addition, the conditions for the BCS-BEC crossover to occur could soon be purposely arranged in the emerging class of superconducting metamaterials [17] whereby the optimization of the proximity effect should prove especially relevant to the purpose.

The paper is organized as follows. Section II sets up the treatment of the proximity effect in terms of the NLPDA equation. Section III presents our numerical results for the profile of the gap parameter under a variety of circumstances from which we are able to extract the temperature dependence of both the pair penetration depth ξ_R and the coherence (healing) length ξ_L on the right and left of the interfaces, respectively. This information is then used for optimizing the proximity effect along the BCS-BEC crossover, and Sec. IV gives our conclusions. Finally, in the Appendix, a summary is given of the numerical procedure that solves the NLPDA equation in one dimension (1D) for the problem at hand.

II. PROXIMITY EFFECT IN TERMS OF THE (INTEGRAL) NLPDA GAP EQUATION

In this section, we briefly recall the structure of the NLPDA equation, that was obtained in Ref. [13] and further analyzed

in Ref. [14], and reduce it to a one-dimensional form that corresponds to the proximity effect of interest when the gap parameter varies across the interface between two superconductors with different critical temperatures. To this end, we will need to specify the shape of the (smooth) variation of the coupling constant across the interface as well as of the external potential which is required to keep the (left plus right) compound system at thermodynamic equilibrium.

A. The NLPDA equation

In Ref. [13], the following (integral) equation for the local gap parameter $\Delta(\mathbf{r})$:

$$-\frac{m}{4\pi a_F}\Delta(\mathbf{r}) = \int d\mathbf{R}\, K(\mathbf{r}-\mathbf{R}|\mathbf{r})\Delta(\mathbf{R}) \tag{1}$$

$$= \int \frac{d\mathbf{Q}}{\pi^3} e^{2i\mathbf{Q}\cdot\mathbf{r}} K(\mathbf{Q}|\mathbf{r})\Delta(\mathbf{Q}) \tag{2}$$

(referred to as the NLPDA equation) was obtained by a suitable coarse-graining procedure applied to the BdG equations. (We set $\hbar = 1$ throughout.) The kernel of this equation reads

$$K(\mathbf{Q}|\mathbf{r}) = \int \frac{d\mathbf{k}}{(2\pi)^3}\left\{\frac{1-2f_F[E_+(\mathbf{k};\mathbf{Q}|\mathbf{r})]}{2E(\mathbf{k};\mathbf{Q}|\mathbf{r})} - \frac{m}{\mathbf{k}^2}\right\}, \tag{3}$$

where m is the fermion mass, $f_F(E) = (e^{E/(k_BT)}+1)^{-1}$ is the Fermi function at temperature T (k_B being the Boltzmann constant),

$$E_\pm(\mathbf{k};\mathbf{Q}|\mathbf{r}) = \sqrt{\left(\frac{\mathbf{k}^2}{2m}+\frac{\mathbf{Q}^2}{2m}-\mu(\mathbf{r})\right)^2 + |\Delta(\mathbf{r})|^2} \pm \frac{\mathbf{k}}{m}\cdot\mathbf{Q}, \tag{4}$$

and $2E(\mathbf{k};\mathbf{Q}|\mathbf{r}) = E_+(\mathbf{k};\mathbf{Q}|\mathbf{r}) + E_-(\mathbf{k};\mathbf{Q}|\mathbf{r})$. In the above expression, $\mu(\mathbf{r}) = \mu - V(\mathbf{r})$ is the local chemical potential in the presence of an external potential $V(\mathbf{r})$ and $|\Delta(\mathbf{r})|$ is the magnitude of the local gap parameter. (As they stand, the above expressions do not include the effects of a magnetic field.) In addition, the kernel,

$$K(\mathbf{R}|\mathbf{r}) = \int \frac{d\mathbf{Q}}{\pi^3} e^{2i\mathbf{Q}\cdot\mathbf{R}} K(\mathbf{Q}|\mathbf{r}), \tag{5}$$

in (real) $\mathbf{R}$-space results from Fourier transforming the kernel (3) in (wave-vector) $\mathbf{Q}$ space.

The left-hand side of the NLPDA equation [in either form (1) or (2)] contains the scattering length a_F for the two-fermion problem. In terms of this quantity, one can form the dimensionless coupling parameter $(k_Fa_F)^{-1}$ that spans the BCS-BEC crossover [2], where $k_F = (3\pi^2 n_0)^{1/3}$ is the Fermi wave vector with (uniform) particle density n_0. This parameter ranges from $(k_Fa_F)^{-1} \lesssim -1$ in the weak-coupling (BCS) regime when $a_F < 0$ to $(k_Fa_F)^{-1} \gtrsim +1$ in the strong-coupling (BEC) regime when $a_F > 0$ across the unitary limit when $|a_F|$ diverges [in practice, the "crossover region" $-1 \lesssim (k_Fa_F)^{-1} \lesssim +1$ is of most interest].

B. The density equation

The NLPDA integral equation (1) [or (2)] is highly nonlinear in the gap parameter Δ. It thus generalizes the linear integral equation adopted in Refs. [3–5] to deal with the proximity effect, which (by construction) was valid only in the vicinity of the superconducting transition T_c^L when Δ is small (with respect to $k_BT_c^L$). The NLPDA equation can then be applied for all temperatures in the superfluid phase and can span the BCS-BEC crossover for arbitrary values of the coupling parameter $(k_Fa_F)^{-1}$ once it is supplemented by the density equation to determine the thermodynamic chemical potential μ,

$$n(\mathbf{r}) = \int \frac{d\mathbf{k}}{(2\pi)^3}\left\{1 - \frac{\xi(\mathbf{k}|\mathbf{r})}{E(\mathbf{k}|\mathbf{r})}\{1-2f[E(\mathbf{k}|\mathbf{r})]\}\right\}, \tag{6}$$

where $\xi(\mathbf{k}|\mathbf{r}) = \frac{\mathbf{k}^2}{2m} - \mu(\mathbf{r})$ and $E(\mathbf{k}|\mathbf{r}) = \sqrt{\xi(\mathbf{k}|\mathbf{r})^2 + |\Delta(\mathbf{r})|^2}$ [13]. The expression (6) holds with a real gap parameter in the absence of currents.

C. Variation of the coupling constant across the interface

In Refs. [3–5] two different values of the interparticle interaction were considered for the semi-infinite systems on the left (L) and right (R) of the interface separating them at $x = 0$. By a similar token, here we attribute two different values of the coupling parameter $(k_Fa_F)^{-1}$ to the half-systems on the left and right of the interface and assume translational invariance on the y-z plane parallel to the interface in such a way that both the external potential $V(x)$ and the gap parameter $\Delta(x)$ depend only on x. To avoid too sharp a behavior about $x = 0$, it is convenient to smooth out the x profile of the coupling parameter over a length σ (on the order of k_F^{-1}) by introducing the model function,

$$g(x) \equiv -\frac{m}{4\pi a_F(x)} = \frac{1}{2}[g_R + g_L + (g_R - g_L)G_\sigma(x)], \tag{7}$$

where $g_L = -m/(4\pi a_F^L)$ and $g_R = -m/(4\pi a_F^R)$ are the asymptotic values on the left and right sides, respectively, of the interface. For most calculations, we will consider the function $G_\sigma(x)$ of the form

$$G_\sigma(x) = \tanh\left(\frac{x}{\sigma}\right); \tag{8}$$

for the sake of comparison, however, we have sometimes utilized also the following function with compact support:

$$G_\sigma(x) = \tanh\left(\frac{\frac{x}{\sigma}}{\sqrt{1-\left(\frac{x}{\sigma}\right)^2}}\right) \qquad \left[\frac{|x|}{\sigma} \leqslant 1\right]$$

$$= \mathrm{sgn}\left(\frac{x}{\sigma}\right) \qquad \left[\frac{|x|}{\sigma} \geqslant 1\right]. \tag{9}$$

A typical profile of $g(x)$ with the choice (8) is shown in Fig. 1(a).

D. Choice of the external potential

The potential $V(x)$, that enters the NLPDA equation (1) [or (2)] and the density equation (6) through the local chemical potential $\mu(x)$, can be modeled in several ways, depending on the experimental conditions one is after. Here, we consider the following choice for $V(x)$.

We assume that the system on the left (right) of the interface extends to $-\infty$ ($+\infty$) such that away from the interface in the bulk region it approaches a homogeneous superconductor with coupling $(k_Fa_F^L)^{-1}$ [$(k_Fa_F^R)^{-1}$] and bulk (asymptotic) value μ_L (μ_R) of the chemical potential. For

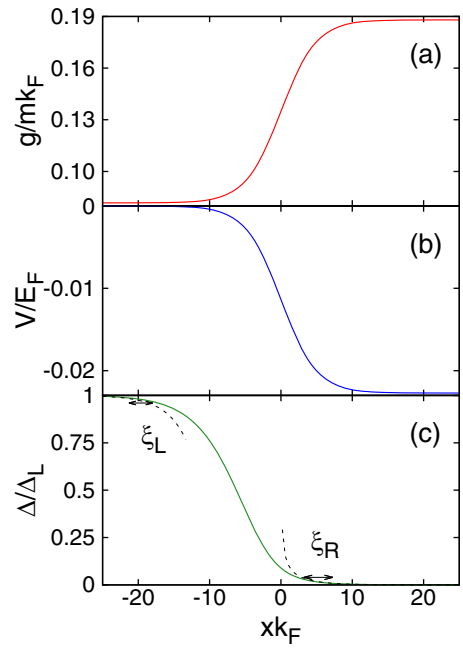

FIG. 1. Characteristic spatial profiles of (a) the coupling constant $g(x)$ of Eq. (7) (in units of mk_F), (b) the external potential $V(x)$ of Eq. (11) [in units of the Fermi energy $E_F = k_F^2/(2m)$], and (c) the gap parameter $\Delta(x)$ (in units of Δ_L) obtained by solving the NLPDA equation in the form (14). For this example, we have taken $(k_F a_F^L)^{-1} = -1.0$ and $(k_F a_F^R)^{-1} = -2.34$ such that $T_c^L/T_F = 0.12$ and $T_c^R/T_F = 0.015$, $T/T_F = 0.09$ such that $T_c^R < T < T_c^L$, $\mu_L/E_F = 0.971$, $\mu_R/E_F = 0.993$, and $\Delta_L/E_F = 0.154$. (Here $T_F = E_F/k_B$ is the Fermi temperature.) We have also taken $\sigma = 5k_F^{-1}$ for the parameter that enters Eqs. (7)–(11). The dashed lines in panel (c) represent the asymptotic expressions (16) and (17) from which ξ_R and ξ_L are extracted at given T.

simplicity, we further assume that the density has the same bulk (asymptotic) value of $n_0 = k_F^3/(3\pi^2)$ on both sides of the interface. At a given temperature, this corresponds to the value of $n(-\infty)$ obtained from Eq. (6) with chemical potential μ_L and $\Delta(-\infty) = \Delta_L$ and to the value of $n(+\infty)$ obtained from Eq. (6) with chemical potential μ_R and $\Delta(+\infty) = \Delta_R$. However, since at equilibrium the thermodynamic chemical potential μ must maintain the same value across the whole system, the situation can be kept thermodynamically stable only in the presence of an external potential $V(x)$, which makes the local chemical potential $\mu(x) = \mu - V(x)$ entering Eq. (6) interpolate smoothly between the asymptotic values of μ_L and μ_R. In analogy with Eq. (7), we write

$$V(x) = \mu - \tfrac{1}{2}[(\mu_R + \mu_L) + (\mu_R - \mu_L)G_\sigma(x)], \qquad (10)$$

whereby $V(-\infty) = \mu - \mu_L$ and $V(+\infty) = \mu - \mu_R$. At a given temperature, the arbitrariness on the value of μ can be eliminated by fixing $\mu = \mu_L$, which corresponds to a homogeneous system with density n_0 and coupling $(k_F a_F^L)^{-1}$. In this way, $V(-\infty) = 0$ and the expression (10) reduces to the form

$$V(x) = \tfrac{1}{2}(\mu_L - \mu_R)[1 + G_\sigma(x)], \qquad (11)$$

which depends on temperature through the temperature dependence of both μ_L and μ_R. In particular, when $T_c^R < T_c^L$ one expects $\mu_L < \mu_R$ such that $V(x) \leqslant 0$ from Eq. (11). A typical profile of $V(x)$ is shown in Fig. 1(b). The potential $V(x)$ thus acts as a barrier that effectively prevents the particles from flowing from the right toward the left of the interface while trying to take advantage of the smaller local value of the chemical potential. Accordingly, close to the interface one expects the local density $n(x)$ to somewhat deviate from its bulk value n_0, possibly leading to a depression on one side and to an enhancement on the other side of the interface. In a condensed-matter system, this situation would correspond to the presence of an electrostatic dipole layer across the boundary surface [18].

E. Solution of the NLPDA equation across the interface

Under the above circumstances, the gap parameter in **Q** space that enters the right-hand side of Eq. (2) reduces to the form

$$\Delta(\mathbf{Q}) = \pi^2 \delta(Q_y)\delta(Q_z)\Delta(Q_x). \qquad (12)$$

Correspondingly, the NLPDA equation (2) simplifies as follows:

$$g(x)\Delta(x) = \int_{-\infty}^{+\infty} \frac{dQ}{\pi} e^{2iQx} K(|Q||x)\Delta(Q), \qquad (13)$$

with the notation of Eq. (7) and where we have set $Q_x \to Q$ in Eq. (13) to shorten the notation. Note that in the expression (13) we have emphasized the fact that the kernel K depends on the magnitude $|Q|$ of Q.

The integral equation (13) can be solved using general method developed in Appendix B of Ref. [14] where the Fourier transform of a function with a given spatial symmetry in D dimensions was calculated in terms of the eigenfunctions of the harmonic oscillator. In the Appendix below this method is further adapted to the present 1D case whereby the gap parameter $\Delta(x)$ is neither symmetric nor antisymmetric across the interface at $x = 0$, and the coupling parameter $g(x)$ depends on x. The end result is the following discretized expression of the 1D-NLPDA integral equation (13) [19]:

$$\begin{aligned} &g\left(\frac{x_j}{\sqrt{2}\lambda}\right)\Delta\left(\frac{x_j}{\sqrt{2}\lambda}\right) \\ &= \frac{1}{y_j}\sum_{n=0}^{N-1}\sum_{j'=1}^{N} i^n S_{jn}^T S_{nj'} K\left(\frac{\lambda|x_{j'}|}{\sqrt{2}}\middle|\frac{x_j}{\sqrt{2}\lambda}\right) \\ &\quad\times \sum_{n'=0}^{N-1}\sum_{j''=1}^{N}(-i)^{n'} S_{j'n'}^T S_{n'j''} y_{j''} \Delta\left(\frac{x_{j''}}{\sqrt{2}\lambda}\right). \end{aligned} \qquad (14)$$

In this expression: (i) $\frac{x_j}{\sqrt{2}\lambda}$ refers to values of x in real space and $\frac{\lambda x_j}{\sqrt{2}}$ to values of Q in wave-vector space, (ii) the points $\{x_j; j = 1, \ldots, N\}$ correspond to the zeros of the (normalized) Hermite polynomial $\mathcal{H}_N(x)$ [cf. Eq. (A16)], (iii) the matrix elements of the orthogonal matrix S are given by Eq. (A10), (iv) the positive definite weights w_j are obtained by the normalization condition (A17) for the eigenvectors of the eigenvalue problem (A16), and (v) the quantity y_j is given by Eq. (A10). The (positive) parameter λ is meant to add extra flexibility to the numerical calculations. The number of points N in the two (x and Q) meshes and the parameter λ

can be varied to achieve optimal convergence of the Fourier transforms from $\Delta(x)$ to $\Delta(Q)$ and vice versa. A typical profile for $\Delta(x)$ obtained in this way is shown in Fig. 1(c).

The discretized version (14) of the 1D-NLPDA equation is solved until self-consistency is achieved by following closely the prescriptions discussed in Appendix B of Ref. [14]. In practice, the values of the gap $\Delta(x)$ are explicitly calculated over a coarse mesh of M points (we have taken $M = 350$ in most calculations). A numerical interpolation is then used to generate the $N(> M)$ values of $\Delta(x)$ needed in Eq. (14) (typically, $N = 30M$ proves sufficient). This interpolation is required to avoid unwanted oscillations of small wavelengths which would be generated otherwise. Finally, the value of the parameter λ entering Eq. (14) is chosen in such a way that the N zeros of the Hermite polynomials extend over a spatial range which is three times wider than that covered by the M points utilized for the profile of $\Delta(x)$ (typically, we have taken $\lambda k_F = 10$). For the needs of the present paper, the self-consistent solution of Eq. (14) has been achieved in a few hundred cases.

III. NUMERICAL RESULTS

The numerical solution of the integral equation (14) has been performed in several cases by varying the coupling constants $(k_F a_F^L)^{-1}$ at the left and $(k_F a_F^R)^{-1}$ at the right of the interface as well as the width σ of the separating barrier. In particular, we have considered the values of $(k_F a_F^L)^{-1} = (-1.0, 0.0)$ such that $T_c^L/T_F = (0.12, 0.50)$, and we have correspondingly adapted the value of $(k_F a_F^R)^{-1}$ such that $T_c^L/T_c^R = (8, 4, 2)$ [20]. In addition, we have taken $k_F\sigma = (2.5, 5.0, 10.0)$ for the choice (8) and $k_F\sigma = 5.0$ for the choice (9) of $G_\sigma(x)$. This wide choice of input parameters will enable us to draw some definite conclusions about the way the proximity effect can be optimized (or, in reverse, depressed).

A. Profile of the gap parameter across the interface under various circumstances

The basic results of the present calculation are represented by the gap profiles $\Delta(x)$ across the interface. Several examples of these profiles are shown in Figs. 2 and 3 for $(k_F a_F^L)^{-1} = -1.0$ and $(k_F a_F^L)^{-1} = 0.0$, respectively, with the choice of $k_F\sigma = 5.0$ for the barrier (8). In each figure, the three panels refer to the cases (a) $T_c^L/T_c^R = 8$, (b) $T_c^L/T_c^R = 4$, and (c) $T_c^L/T_c^R = 2$. In each panel, several temperatures are further considered according to the expression,

$$\frac{T}{T_c^L} = \nu + (1-\nu)\frac{T_c^R}{T_c^L} \qquad (0 \leqslant \nu \leqslant 1), \tag{15}$$

such that $T = T_c^R$ for $\nu = 0$ and $T = T_c^L$ for $\nu = 1$. In particular, in Figs. 2 and 3 we have chosen the values of $\nu = (0.05, 0.25, 0.50, 0.75, 0.95)$.

It is also interesting to compare the gap profiles $\Delta(x)$ for different shapes of the barrier. This is performed in Fig. 4 where several values of the barrier width σ are used for the choice (8) and a single value of σ is considered for the choice (9). In particular, panel (b) of Fig. 4 shows that, on the right side of the interface, the gap profile is essentially independent from the shape of the barrier. This result gives us confidence that the values of the pair penetration depth ξ_R, that we will extract from $\Delta(x)$ for $x > 0$ to characterize the proximity effect, will not appreciably depend on a specific choice of the barrier. In addition, this finding (about a well-defined gap profile which is present on the normal side of the interface) could be used to identify definite values for the effective boundary conditions across the interface on the gap parameter and its derivative, which may be then adopted in local (differential) approaches to the problem. For the sake of definiteness, in what follows we limit ourselves to consider a barrier specified by the form (8) with $k_F\sigma = 5.0$.

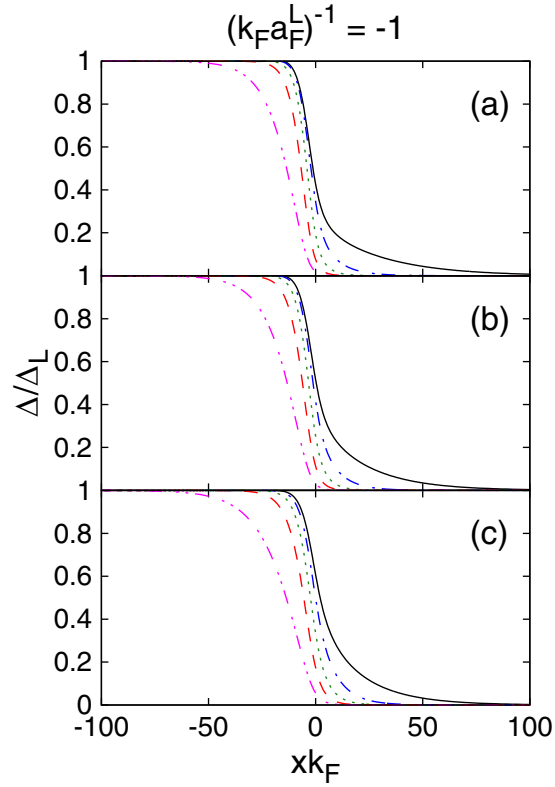

FIG. 2. Gap profiles $\Delta(x)/\Delta_L$ for $(k_F a_F^L)^{-1} = -1.0$ when (a) $T_c^L/T_c^R = 8$, (b) $T_c^L/T_c^R = 4$, and (c) $T_c^L/T_c^R = 2$. The various curves refer to different temperatures chosen according to the expression (15), where $\nu = 0.05$ (full line), $\nu = 0.25$ (dashed-dotted line), $\nu = 0.50$ (dotted line), $\nu = 0.75$ (dashed line), and $\nu = 0.95$ (dashed-double-dotted line).

B. Asymptotic behavior of the gap parameter on both sides of the interface

Out of the numerical results for $\Delta(x)$ like those reported in Figs. 2 and 3, one can extract both the pair penetration depth ξ_R and the coherence (healing) length ξ_L according to the following procedure. At a given temperature T, we fit the behavior of $\Delta(x;T)$ for $k_F x \gg 1$ through the expression,

$$\Delta(x;T) \sim \frac{\gamma_R(T) e^{-x/\xi_R(T)}}{x^{\mathcal{D}-2+\eta}} + \Delta_R(T), \tag{16}$$

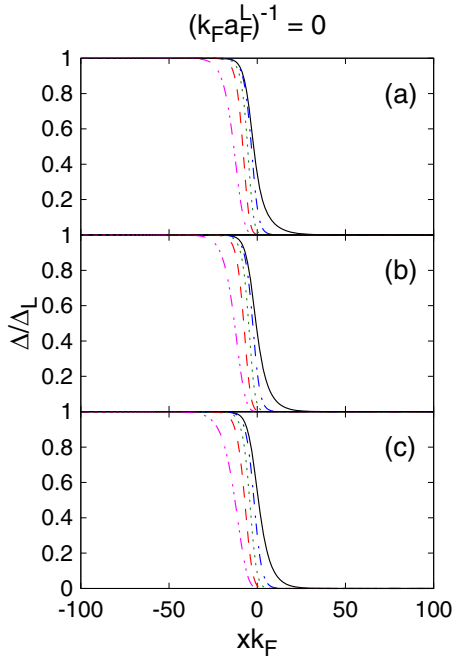

FIG. 3. Gap profiles $\Delta(x)/\Delta_L$ for $(k_F a_F^L)^{-1} = 0.0$ when (a) $T_c^L/T_c^R = 8$, (b) $T_c^L/T_c^R = 4$, and (c) $T_c^L/T_c^R = 2$. Conventions for the various curves are the same as in Fig. 2.

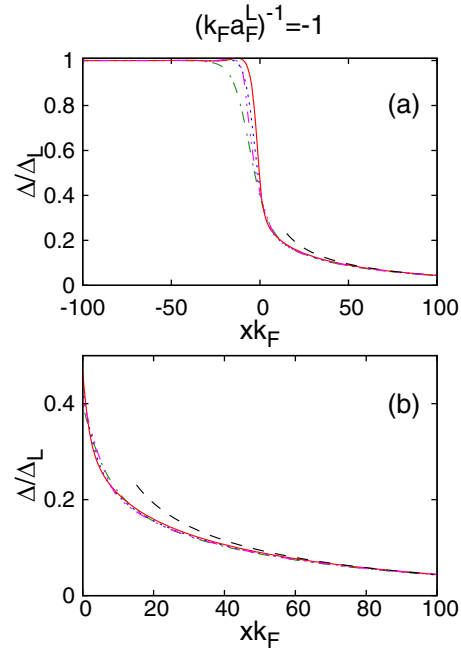

FIG. 4. The gap profile $\Delta(x)/\Delta_L$ for $(k_F a_F^L)^{-1} = -1.0$, $T_c^L/T_c^R = 8$, and $T = 1.04T_c^R$ is shown for several values of the barrier width σ of Eq. (8): $k_F\sigma = 2.5$ (full line), $k_F\sigma = 5.0$ (dotted line), and $k_F\sigma = 10.0$ (dashed-dotted line). Also reported are the results for the choice (9) with $k_F\sigma = 5.0$ (dashed-double-dotted line) and of the fitting (18) (dashed line)—see below. Panel (a) shows the whole profile of $\Delta(x)$ both on the left and on the right of the interface, whereas panel (b) focuses on the right side of the interface from which the pair penetration depth ξ_R of interest is extracted.

whereas for $k_F x \ll -1$ we make use of the specular expression,

$$\Delta(x;T) \sim \Delta_L(T) - \frac{\gamma_L(T) e^{x/\xi_L(T)}}{|x|^{\mathcal{D}-2+\eta}}. \tag{17}$$

In all fits that we have performed, it turns out that the optimal value of $\mathcal{D}+\eta$ is 2.5. We have then set $\eta = 0$ and interpreted $\mathcal{D} = 2.5$ as an effective dimensionality, which is intermediate between $D = 2$ of the planar boundary surface separating the left (L) and right (R) superconductors and $D = 3$ of the space in which this surface is embedded. Note that the expressions (16) and (17) correspond to the generic behavior of the correlation function for the order parameter in a homogeneous medium [21] and are here recovered by the spatial behavior of the order parameter itself for the inhomogeneous problem we are considering [22]. In the expressions (16) and (17), note also the presence of the temperature-dependent (and positive definite) prefactors $\gamma_R(T)$ and $\gamma_L(T)$, which are needed for obtaining accurate fits of the asymptotic gap profiles.

C. Optimizing the proximity effect in terms of ξ_R

Figure 5 shows the results for $\xi_R(T)$ obtained from a fit of the form (16) for the coupling values of $(k_F a_F^L)^{-1} = -1.0$ (upper panel) and $(k_F a_F^L)^{-1} = 0.0$ (lower panel). In each panel, three different cases are reported with $T_c^R/T_c^L = 1/8$, $T_c^R/T_c^L = 1/4$, and $T_c^R/T_c^L = 1/2$. For both couplings of the left superconductor, it is seen that ξ_R attains larger values as soon as the coupling of the right superconductor differs appreciably from that of the left superconductor. This implies that the relevance of the proximity effect is amplified when the bulk values of Δ_L and Δ_R differ appreciably from each other, a criterion that could be exploited in practice to optimize the spatial extension of the proximity effect. For the sake of example, typical values of Δ_L and Δ_R at zero temperature are reported in Table I for the cases of interest.

When comparing the sets of values for ξ_R that correspond to $(k_F a_F^L)^{-1} = -1.0$ and $(k_F a_F^L)^{-1} = 0.0$ as reported in panels (a) and (b) of Fig. 5, respectively, one notes that those for $(k_F a_F^L)^{-1} = -1.0$ result always larger than those for $(k_F a_F^L)^{-1} = 0.0$. This is in line with the fact that, for a homogeneous system, the Cooper pair size $\xi_{\rm pair}$ is smaller for $(k_F a_F^L)^{-1} = 0.0$ (where $k_F\xi_{\rm pair} = 1.1$) than for $(k_F a_F^L)^{-1} = -1.0$ (where $k_F\xi_{\rm pair} = 3.4$) [23] such that the leakage region on the normal side of the interface associated with the proximity effect should correspondingly be smaller. On the other hand, one should also recall that, in absolute value, the range of temperatures over which the proximity effect can occur increases from $(k_F a_F^L)^{-1} = 0.0$ to $(k_F a_F^L)^{-1} = -1.0$ to the extent that the corresponding critical temperature T_c^L is higher when $(k_F a_F^L)^{-1} = 0.0$. Optimizing the proximity effect may thus require one to compromise between these two contrasting behaviors, depending on the physical circumstances of interest.

D. Limiting behaviors for the temperature dependence of ξ_R

The numerical results for $\xi_R(T)$ reported in Fig. 5 can be further analyzed for temperatures close enough to T_c^R and

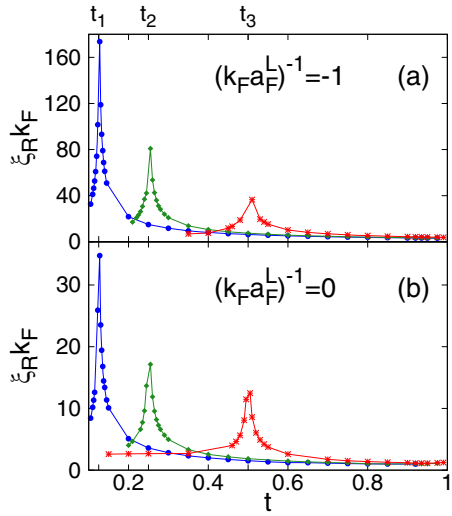

FIG. 5. The pair penetration depth ξ_R (in units of k_F^{-1}) is shown vs the reduced temperature $t = T/T_c^L$ for the coupling values (a) $(k_F a_F^L)^{-1} = -1.0$ and (b) $(k_F a_F^L)^{-1} = 0.0$. In each panel, three cases are reported for $T_c^R/T_c^L = t_1 = 1/8$ (dots), $T_c^R/T_c^L = t_2 = 1/4$ (diamonds), and $T_c^R/T_c^L = t_3 = 1/2$ (stars). (The lines are guides to the eye.)

T_c^L. To this end, we resort to the analytic results that were obtained in Ref. [8] for the extreme weak-coupling (BCS) limit only and utilize them for stronger couplings reaching the unitary limit in order to fit the temperature dependence of ξ_R and ξ_L obtained above out of the expressions (16) and (17). Accordingly, we represent the temperature dependence of ξ_R both close to T_c^R and close to T_c^L (as well as of ξ_L close to T_c^L) in the following way:

$$\xi_R(T) = \frac{A_R^{(+)}}{\sqrt{T - T_c^R}} \quad \left[T \gtrsim T_c^R\right], \tag{18}$$

$$\xi_R(T) = \frac{A_R^{(-)}}{\sqrt{T_c^R - T}} \quad \left[T \lesssim T_c^R\right], \tag{19}$$

$$\xi_R(T) = \frac{B_R}{T} \quad \left[T_c^R \ll T \lesssim T_c^L\right], \tag{20}$$

$$\xi_L(T) = \frac{A_L^{(-)}}{\sqrt{T_c^L - T}} \quad \left[T \lesssim T_c^L\right], \tag{21}$$

where "$\gtrsim$" and "$\lesssim$" signify "in the vicinity of" and "$\ll$" signifies "well above than."

TABLE I. Values of Δ_L and Δ_R (in units of the Fermi energy E_F) at zero temperature for the couplings of interest [20].

$(k_F a_F^L)^{-1}$	$(k_F a_F^R)^{-1}$	T_c^L/T_F	T_c^R/T_F	Δ_L/E_F	Δ_R/E_F
−1.0	−2.36	0.12	0.015	0.20	0.026
−1.0	−1.92	0.12	0.030	0.20	0.053
−1.0	−1.48	0.12	0.060	0.20	0.104
0.0	−1.45	0.50	0.063	0.69	0.108
0.0	−1.00	0.50	0.125	0.69	0.208
0.0	−0.53	0.50	0.250	0.69	0.388

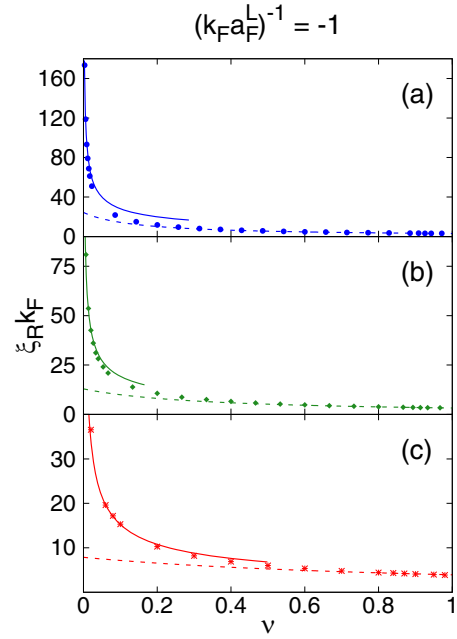

FIG. 6. The pair penetration depth ξ_R (in units of k_F^{-1}) is reported vs the variable ν of Eq. (15) for $(k_F a_F^L)^{-1} = -1.0$, in the three cases when $T_c^L/T_c^R = 8$ (dots: upper panel), $T_c^L/T_c^R = 4$ (diamonds: middle panel), and $T_c^L/T_c^R = 2$ (stars: lower panel). In addition, fits to these symbols are obtained with the expressions (18) close to T_c^R (full lines) and (20) close to T_c^L (dashed lines).

The results of these fits for ξ_R are shown in Fig. 6 for $(k_F a_F^L)^{-1} = -1.0$ and in Fig. 7 for $(k_F a_F^L)^{-1} = 0.0$ where in each case $T_c^L/T_c^R = 8$ (upper panel), $T_c^L/T_c^R = 4$ (middle panel), and $T_c^L/T_c^R = 2$ (lower panel). Note that, to draw

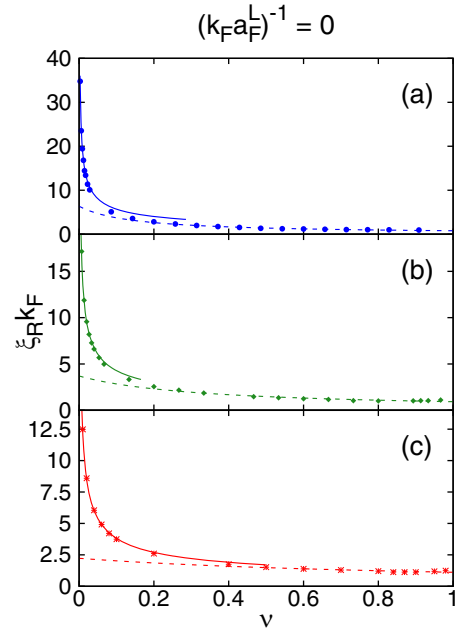

FIG. 7. Pair penetration depth ξ_R (in units of k_F^{-1}) vs the variable ν of Eq. (15) for $(k_F a_F^L)^{-1} = 0.0$. Conventions and symbols are the same as in Fig. 6.

TABLE II. The coefficients of the expressions (18) and (19), obtained by fits through the numerical values of ξ_R and ξ_L over the appropriate temperature ranges, are reported in a few cases of interest. Here, $A_R^{(\pm)}$ is in units of $\sqrt{\frac{T_c^R}{2mT_F}}$, $A_L^{(-)}$ is in units of $\sqrt{\frac{T_c^L}{2mT_F}}$, and B_R is in units of T_c^R.

$(k_F a_F^L)^{-1}$	$(k_F a_F^R)^{-1}$	T_c^L/T_F	T_c^R/T_F	$A_R^{(+)}$	$A_R^{(-)}$	B_R	$A_L^{(-)}$
−1.0	−2.36	0.12	0.015	192.7	119.7	198.9	5.7
−1.0	−1.92	0.12	0.030	60.9	38.5	74.7	5.6
−1.0	−1.48	0.12	0.060	19.7	15.4	32.1	5.7
0.0	−1.45	0.50	0.063	19.1	14.5	26.1	1.2
0.0	−1.00	0.50	0.125	6.6	5.4	9.8	1.2
0.0	−0.53	0.50	0.250	2.4	2.3	4.3	1.2

these three different cases over the same horizontal scale, we have identified the reduced temperature T/T_c^L in terms of the variable ν of Eq. (15) such that $T = T_c^R$ when $\nu = 0$ and $T = T_c^L$ when $\nu = 1$. In each case, the numerical values for ξ_R (symbols) are fitted close to T_c^R via the expression (18) (full lines) and close to T_c^L via the expression (20) (dashed lines). The values of all coefficients entering the expressions (18)–(21) are reported in Table II for all cases considered in Figs. 6 and 7. These results confirm the occurrence of a two-slope dependence for the temperature-dependent pair penetration depth (corresponding to the full and dashed lines, respectively, in Figs. 6 and 7) as was anticipated in the Introduction. In addition, these results can be regarded as assessing the quite good accuracy of our numerical calculations.

E. Density profile across the interface

As anticipated in Sec. II D, the presence of the external potential (11) is expected to somewhat modify the density profile near the interface, despite the fact that the bulk density is assumed to have the same value of n_0 on both sides of the interface. To determine the amount of this effect, we have evaluated the density profile $n(x)$ by performing the wave-vector integration in the expression (6) in spherical coordinates with the local values of $\Delta(x)$ and $\mu(x)$ as they vary across the interface. The results of this calculation are shown in Fig. 8 for $(k_F a_F^L)^{-1} = -1.0$ and using a barrier specified by the form (8) with $k_F\sigma = 5.0$ when $T_c^L/T_c^R = 8$ (upper panel), $T_c^L/T_c^R = 4$ (middle panel), and $T_c^L/T_c^R = 2$ (lower panel). In each panel, different curves correspond to different temperatures taken between T_c^R and T_c^L with the same convention as in Fig. 2. Note that, close to the interface in all cases, small (less than 3%) deviations occur for $n(x)$ from its bulk value of n_0. In addition, at the lowest temperature (which in each panel is 95% close to T_c^R over the interval $T_c^L - T_c^R$), the depression in $n(x)$ on the left side of the interface is accompanied by a corresponding enhancement on the right side of the interface (full curves). This dip-and-peak profile is soon washed out for increasing temperature.

F. Width of the kernel of the NLPDA equation across the interface

The spatial width of the kernel K of the NLPDA equation (1) was shown in Ref. [14] to correspond to the Cooper pair

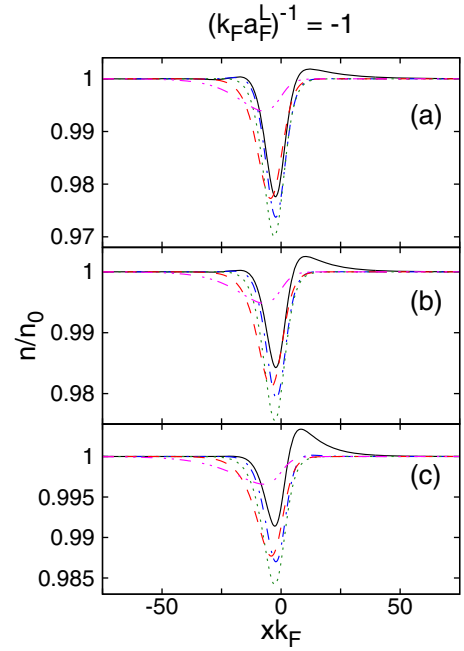

FIG. 8. Density profiles (in units of the bulk density n_0) for $(k_F a_F^L)^{-1} = -1.0$ when (a) $T_c^L/T_c^R = 8$, (b) $T_c^L/T_c^R = 4$, and (c) $T_c^L/T_c^R = 2$. Conventions for the various curves are the same as in Fig. 2.

size over the whole coupling-vs-temperature phase diagram up to the critical temperature. This result was obtained using the values of Δ and μ that correspond to a homogeneous system for given temperature and coupling. In the present context, however, where both $\Delta(x)$ and $\mu(x)$ vary across the interface at $x = 0$ in the temperature interval $T_c^R < T < T_c^L$ of interest, the width of the kernel K of the 1D-NLPDA equation is also expected to depend on x.

To extract this dependence, we consider the kernel in real space [24],

$$K(x|x_0) = \int_{-\infty}^{+\infty} \frac{dQ}{\pi} e^{2iQx} K(|Q||x_0), \tag{22}$$

which is an even function of x and is calculated according to an expression similar to Eq. (A13) of the Appendix. Here, x_0 is the spatial point whereby the values of the local gap $\Delta(x_0)$ and chemical potential $\mu(x_0)$ enter the kernel $K(|Q||x_0)$ in Eq. (13). A typical profile of $K(x|x_0)$ is shown in Fig. 9.

The width of $K(x|x_0)$ is then determined for given x_0 by considering the function,

$$F(X|x_0) = \int_{x_{\max}}^{+X} dx\, K(x|x_0), \tag{23}$$

where $x_{\max} > 0$ is the position of the maximum on the right in the profile of $K(x|x_0)$ (which also depends on x_0 and has to be determined in each case). The function (23) is found to converge asymptotically to a finite value of $F(\infty|x_0)$ when $X \to \infty$. We thus look for the value of $\bar{X}(x_0)$ of X such that $F(\bar{X}|x_0)$ differs from $F(\infty|x_0)$ by, say, 10%. By our definition, the width of the kernel K is identified with *twice* the value of $\bar{X}(x_0)$ for any given x_0.

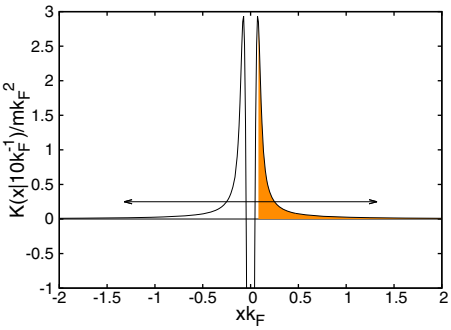

FIG. 9. Typical spatial profile of the kernel $K(x|x_0)$ of the 1D-NLPDA equation (in units of mk_F^2) for $(k_F a_F^L)^{-1} = -1.0$, $T_c^L/T_c^R = 8$, $x_0 k_F = 10$, and temperature halfway between T_c^R and T_c^L. The shaded area corresponds to the region over which the integral (23) is calculated, whereas the double arrow represents the width $2\bar{X}(x_0)$ of the kernel as identified by the procedure described in the text.

Figure 10 shows the quantity $\bar{X}(x_0)$ determined in this way vs x_0 for the sake of example when $(k_F a_F^L)^{-1} = -1.0$ and $T_c^L/T_c^R = (8, 4, 2)$. In each case, the various curves refer to different temperatures according to the conventions of Fig. 2. Note how, in each case, the shape of $\bar{X}(x_0)$ resembles a smoothed step function, which rises from $\bar{X}(-\infty)$ to $\bar{X}(+\infty) > \bar{X}(-\infty)$ within a narrow interval on the order of the variation of the function $G_\sigma(x)$ entering Eqs. (7) and (11).

In addition, in Fig. 11 we have collected the values of $\bar{X}(-\infty)$ and $\bar{X}(+\infty)$ from the three panels of Fig. 10 and displayed them as functions of the absolute temperature T. It turns out that $\bar{X}(-\infty)$ on the extreme left and $\bar{X}(+\infty)$ on the extreme right of the interface are both decreasing functions of T. In particular, $\bar{X}(-\infty)$ decreases by about 10 % when T/T_c^L varies from 0.125 to 1, in line with what was found in Ref. [12] for the temperature evolution of the Cooper pair size *below* T_c in the homogeneous case at the mean-field level. On the other hand, $\bar{X}(+\infty)$ decreases more significantly over the same temperature interval, which would now correspond to temperatures *above* T_c in the homogeneous case for which it can be calculated only once pairing fluctuations beyond the mean field are properly included [12]. Note, finally, that (twice) the values of $\bar{X}(+\infty)$ on the right of the interface are always smaller than the corresponding values of the pair penetration depth ξ_R reported in Fig. 6 for the same coupling and temperature interval thereby giving definite support to the internal consistency of the procedure we have used for identifying ξ_R.

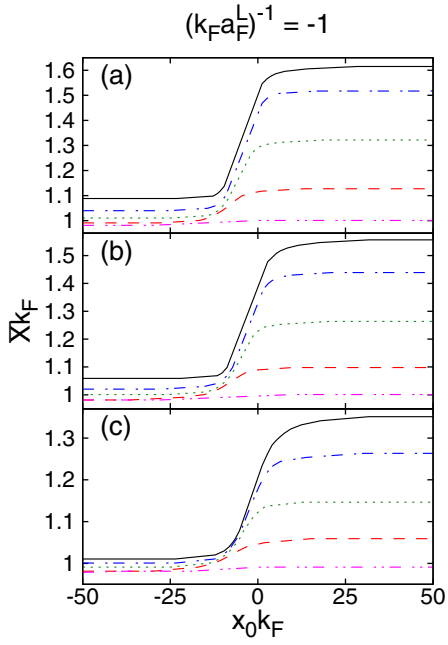

FIG. 10. The quantity $\bar{X}(x_0)$ [such that $2\bar{X}(x_0)$ identifies the width of the kernel of the 1D-NLPDA equation] is shown vs x_0 for $(k_F a_F^L)^{-1} = -1.0$ when (a) $T_c^L/T_c^R = 8$, (b) $T_c^L/T_c^R = 4$, and (c) $T_c^L/T_c^R = 2$. Conventions for the various curves are the same as in Fig. 2.

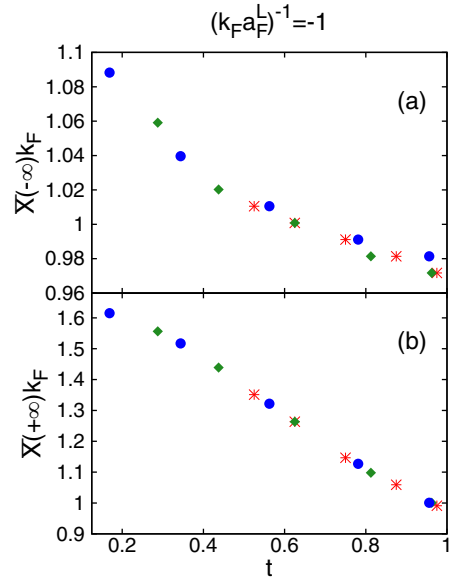

FIG. 11. The values of (a) $\bar{X}(-\infty)$ and (b) $\bar{X}(+\infty)$ collected from Fig. 10 are shown vs $t = T/T_c^L$. Dots, diamonds, and stars refer to the values reported in panels (a)–(c), respectively, of Fig. 10.

IV. CONCLUDING REMARKS

In this paper, we have examined theoretically the proximity effect at the interface between two superconductors with different critical temperatures under a variety of circumstances. To the extent that the size of the Cooper pairs represents a crucial ingredient for the proximity effect, we have been able to vary this size appreciably by making the interparticle coupling for both superconductors to vary along the BCS-BEC crossover (although always remaining on the BCS side of unitarity, which is where the Cooper pair size is comparable with the interparticle distance). We have also been able to consider temperatures quite close (up to 99%) to the critical temperature of either superconductor as well as to modify the shape of the interface separating the two superconductors in order to assess the physical robustness of the calculations.

In this way, from the numerical profiles of the inhomogeneous gap parameter $\Delta(x)$ we have been able to extract the

pair penetration depth ξ_R on the normal (by our convention, the right) side of the interface as a function of both coupling and temperature. This was performed in such an accurate way that the temperature dependence of ξ_R was always found to match the behaviors expected from the analytic estimates made some time ago in Ref. [8] (although in that reference only for what would today be referred to as the BCS limit of the BCS-BEC crossover). On the basis of the values attained by ξ_R under various physical circumstances, we have also proposed a criterion for optimizing the occurrence of the proximity effect.

All of this has been possible because the profiles $\Delta(x)$ of the gap parameter have been obtained by solving numerically the NLPDA integral equation in the form (14) instead of solving the much more demanding BdG differential equations from which the NLPDA equation was derived in Ref. [13] to start with. To this end, we have utilized the method recently provided in Ref. [14] for solving the NLPDA equation in terms of a novel efficient algorithm for calculating the Fourier transforms. In Ref. [14] it was further tested that using the NLPDA instead of the BdG approach not only provides a considerable gain in memory storage, but also results in a large reduction of computational time (which was there quantified in a factor of about 10^2 for the case of an isolated vortex throughout the BCS-BEC crossover for which the solution of the BdG equations is also available [25]).

Given the flexibility of the theoretical approach we have adopted, one may hope that the present paper could stimulate a revival of the experiments that adopt similar geometry and physical arrangements, in particular, by extending the work of Ref. [11] in a systematic way. In addition, when a stationary current would be added to the present calculation (possibly in the presence of a sandwich of different superconductors), the local profile of the gap parameter associated with the proximity effect could be experimentally measured by tunneling spectroscopy as was performed in Ref. [26].

ACKNOWLEDGMENT

We are indebted to P. Pieri for discussions about the choice (11) of the external potential.

APPENDIX: METHOD FOR THE NUMERICAL SOLUTION OF THE 1D-NLPDA EQUATION

An efficient method to solve numerically the [**Q**-version (2) of the] NLPDA equation was set up in Appendix B of Ref. [14] in any dimension D. The method rests on the peculiar properties of the Fourier transform of the wave functions of the D-dimensional harmonic oscillator when expressed in terms of the generalized Laguerre polynomials for a gap parameter $\Delta(\mathbf{r})$ with a given spatial symmetry.

For the 1D geometry of the proximity effect of interest to the present paper where the gap parameter $\Delta(x)$ has both even and odd components in $x \leftrightarrow -x$, one could thus split into even and odd components both the coupling parameter $g(x)$ of Eq. (7) and the product $g(x)\Delta(x)$ which appears on the left-hand side of Eq. (13), to end up with two coupled equations for the even and odd components of $\Delta(x)$. Given the simple 1D geometry of interest, however, one can most simply rephrase the method developed in Appendix B of Ref. [14] in terms of Hermite polynomials instead of generalized Laguerre polynomials. For completeness, in the following we will concisely report the relevant expressions needed to solve numerically Eq. (13), which are obtained by rephrasing in terms of Hermite polynomials the essential steps described in Appendix B of Ref. [14], to which we refer the reader for additional details.

Consider a 1D harmonic oscillator with mass $m = 2\lambda^2$ and frequency $\omega = 1$ (with the parameter λ introduced to give additional flexibility to the numerical calculations). Its (normalized) eigenfunctions have the form

$$\psi_n(x) = (2\lambda^2)^{1/4} e^{-\lambda^2 x^2} \mathcal{H}_n(\sqrt{2}\lambda x), \tag{A1}$$

with

$$\mathcal{H}_n(x) = \frac{1}{\pi^{1/4}\sqrt{2^n n!}} H_n(x), \tag{A2}$$

where $H_n(x)$ $(n = 0, 1, \ldots)$ are Hermite polynomials such that

$$\int_{-\infty}^{+\infty} dx\, e^{-x^2} \mathcal{H}_n(x)\mathcal{H}_{n'}(x) = \delta_{nn'}. \tag{A3}$$

The corresponding Fourier transform is given by

$$\begin{aligned}\tilde{\psi}_n(Q) &= \int_{-\infty}^{+\infty} dx\, e^{-2iQx} \psi_n(x) \\ &= (-i)^n \left(\frac{2\pi^2}{\lambda^2}\right)^{1/4} e^{-Q^2/\lambda^2} \mathcal{H}_n\left(\frac{\sqrt{2}Q}{\lambda}\right)\end{aligned} \tag{A4}$$

(for clarity, in this Appendix we add a tilde to the symbol of the Fourier transform).

Owing to the property of the Fourier transforms,

$$\int_{-\infty}^{+\infty} dx\, \psi_n(x)\Delta(x) = \int_{-\infty}^{+\infty} \frac{dQ}{\pi}\, \tilde{\psi}_n^*(Q)\tilde{\Delta}(Q), \tag{A5}$$

we can write in terms of the expressions (A1) and (A4),

$$\begin{aligned}&\int_{-\infty}^{+\infty} dx\, e^{-x^2} \mathcal{H}_n(x) e^{x^2/2} \Delta\left(\frac{x}{\sqrt{2}\lambda}\right) \\ &\quad = \frac{i^n\lambda}{\sqrt{\pi}} \int_{-\infty}^{+\infty} dx\, e^{-x^2} \mathcal{H}_n(x) e^{x^2/2} \tilde{\Delta}\left(\frac{\lambda x}{\sqrt{2}}\right).\end{aligned} \tag{A6}$$

The above expressions can be cast in an approximate form useful for numerical calculations by introducing a Gaussian quadrature of the form [cf. Eq. (A3)]

$$\int_{-\infty}^{+\infty} dx\, e^{-x^2} \mathcal{H}_n(x)\mathcal{H}_{n'}(x) = \sum_{j=1}^{N} w_j \mathcal{H}_n(x_j)\mathcal{H}_{n'}(x_j) = \delta_{nn'}, \tag{A7}$$

where the points $\{x_j; j = 1, \ldots, N\}$ and the (positive definite) weights $\{w_j; j = 1, \ldots, N\}$ have to be determined. We then write for the left-hand side of Eq. (A6),

$$\int_{-\infty}^{+\infty} dx\, e^{-x^2} \mathcal{H}_n(x) e^{x^2/2} \Delta\left(\frac{x}{\sqrt{2}\lambda}\right) \simeq \sum_{j=1}^{N} S_{nj} y_j \Delta\left(\frac{x_j}{\sqrt{2}\lambda}\right), \tag{A8}$$

as well as for the right-hand side of Eq. (A6),

$$\int_{-\infty}^{+\infty} dx\, e^{-x^2}\mathcal{H}_n(x)e^{x^2/2}\tilde{\Delta}\left(\frac{\lambda x}{\sqrt{2}}\right) \simeq \sum_{j=1}^{N} S_{nj}\, y_j\, \tilde{\Delta}\left(\frac{\lambda x_j}{\sqrt{2}}\right), \tag{A9}$$

where we have introduced the quantities,

$$S_{nj} = \mathcal{H}_n(x_j)\sqrt{w_j}, \qquad y_j = e^{x_j^2/2}\sqrt{w_j}, \tag{A10}$$

such that

$$\sum_{j=1}^{N} S_{nj}\, S^T_{jn'} = \delta_{nn'}, \qquad \sum_{n=0}^{N-1} S^T_{jn} S_{nj'} = \delta_{jj'}. \tag{A11}$$

Entering the results (A8) and (A9) into Eq. (A6), we obtain approximately,

$$\sum_{j=1}^{N} S_{nj}\, y_j\, \Delta\left(\frac{x_j}{\sqrt{2}\lambda}\right) = \frac{i^n\lambda}{\sqrt{\pi}} \sum_{j=1}^{N} S_{nj}\, y_j\, \tilde{\Delta}\left(\frac{\lambda x_j}{\sqrt{2}}\right), \tag{A12}$$

from which we can extract, alternatively,

$$\Delta\left(\frac{x_j}{\sqrt{2}\lambda}\right) = \frac{\lambda}{\sqrt{\pi}\, y_j} \sum_{n=0}^{N-1}\sum_{j=1}^{N} i^n\, S^T_{jn} S_{nj'} y_{j'}\, \tilde{\Delta}\left(\frac{\lambda x_{j'}}{\sqrt{2}}\right), \tag{A13}$$

and

$$\tilde{\Delta}\left(\frac{\lambda x_j}{\sqrt{2}}\right) = \frac{\sqrt{\pi}}{\lambda y_j} \sum_{n=0}^{N-1}\sum_{j=1}^{N} (-i)^n\, S^T_{jn} S_{nj'} y_{j'}\, \Delta\left(\frac{x_{j'}}{\sqrt{2}\lambda}\right), \tag{A14}$$

where $\frac{x_j}{\sqrt{2}\lambda}$ refers to values of x and $\frac{\lambda x_j}{\sqrt{2}}$ refers to values of Q with the two meshes of x and Q points closely interlinked with each other. In these expressions, both the number of points N in the two meshes and the parameter λ can be varied to achieve optimal convergence of the Fourier transform from $\Delta(x)$ to $\Delta(Q)$ (and vice versa). The two results (A13) and (A14) taken together provide an efficient algorithm to calculate the Fourier transform of any function in 1D.

There remains to determine the sets of points $\{x_j\}$ and the corresponding weights $\{w_j\}$ that appear in the definitions (A10). To this end, we take advantage of the recursion relation [27],

$$\sqrt{n+1}\mathcal{H}_{n+1}(x) - \sqrt{2}x\mathcal{H}_n(x) + \sqrt{n}\mathcal{H}_n(x) = 0, \tag{A15}$$

which we apply recursively from $n = 0$ to $n = N-1$ and choose for x the N values $\bar{x}$ such that $\mathcal{H}_N(\bar{x}) = 0$. In this way, we end up with the following $N \times N$ eigenvalue problem:

$$\begin{pmatrix} -\sqrt{2}\bar{x} & 1 & 0 & \cdots & & \\ 1 & -\sqrt{2}\bar{x} & \sqrt{2} & 0 & \cdots & \\ 0 & \sqrt{2} & -\sqrt{2}\bar{x} & \sqrt{3} & 0 & \cdots \\ \cdots & \cdots & \cdots & \cdots & \cdots & \cdots \\ & \cdots & 0 & \sqrt{N-2} & -\sqrt{2}\bar{x} & \sqrt{N-1} \\ & & \cdots & 0 & \sqrt{N-1} & -\sqrt{2}\bar{x} \end{pmatrix} \begin{pmatrix} \mathcal{H}_0(\bar{x}) \\ \mathcal{H}_1(\bar{x}) \\ \mathcal{H}_2(\bar{x}) \\ \cdots \\ \mathcal{H}_{N-2}(\bar{x}) \\ \mathcal{H}_{N-1}(\bar{x}) \end{pmatrix} = \begin{pmatrix} 0 \\ 0 \\ 0 \\ \cdots \\ 0 \\ 0 \end{pmatrix}. \tag{A16}$$

By diagonalizing the real and symmetric matrix on the left-hand side of Eq. (A16), we obtain eventually the N (distinct) eigenvalues $\bar{x}_j$ (with $j = 1, 2, \ldots, N$) and the corresponding N eigenvectors $[\mathcal{H}_0(\bar{x}_j), \mathcal{H}_1(\bar{x}_j), \mathcal{H}_2(\bar{x}_j), \ldots, \mathcal{H}_{N-2}(\bar{x}_j), \mathcal{H}_{N-1}(\bar{x}_j)]$, whose normalization condition,

$$\sum_{n=0}^{N-1} \mathcal{H}_n(\bar{x}_j)\mathcal{H}_n(\bar{x}_j) = \frac{\delta_{jj'}}{w_j} \tag{A17}$$

provides the weights w_j according to the second identity in Eq. (A11).

The above results can be used to solve the 1D-NLPDA integral equation (13) with variable coupling constant $g(x)$ in an efficient way. The ensuing discretized form of this integral equation is reported in Eq. (14) of the main text.

[1] I. Žutić, A. Matos-Abiague, B. Scharf, H. Dery, and K. Belashchenko, Proximitized materials, arXiv:1805.07942 [Materials Today (to be published)].

[2] G. C. Strinati, P. Pieri, G. Röpke, P. Schuck, and M. Urban, The BCS-BEC crossover: From ultra-cold Fermi gases to nuclear systems, Phys. Rep. **738**, 1 (2018).

[3] P. G. de Gennes, Boundary effects in superconductors, Rev. Mod. Phys. **36**, 225 (1964).

[4] P. G. de Gennes, *Superconductivity of Metals and Alloys* (Benjamin, New York, 1966), Chap. 7.

[5] G. Deutscher and P. G. de Gennes, in *Superconductivity*, edited by R. D. Parks (Dekker, New York, 1969), Vol. 2, p. 1005.

[6] T. M. Klapwijk, Proximity effect from an Andreev perspective, J. Supercond. **17**, 593 (2004), and references therein.

[7] G. Deutscher, Andreev-Saint-James reflections: A probe of cuprate superconductors, Rev. Mod. Phys. **77**, 109 (2005).

[8] V. G. Kogan, Coherence length of a normal metal in a proximity system, Phys. Rev. B **26**, 88 (1982).

[9] G. Eilenberger, Transformation of Gorkov's equation for type II superconductors into transport-like equations, Z. Phys. **214**, 195 (1968).

[10] K. D. Usadel, Generalized diffusion equation for superconducting alloys, Phys. Rev. Lett. **25**, 507 (1970).

[11] E. Polturak, G. Koren, D. Cohen, E. Aharoni, and G. Deutscher, Proximity effect in $YBa_2Cu_3O_7/Y_{0.6}Pr_{0.4}Ba_2Cu_3O_7/YBa_2Cu_3O_7$ Junctions, Phys. Rev. Lett. **67**, 3038 (1991).

[12] F. Palestini and G. C. Strinati, Temperature dependence of the pair coherence and healing lengths for a fermionic superfluid

throughout the BCS-BEC crossover, Phys. Rev. B **89**, 224508 (2014).

[13] S. Simonucci and G. C. Strinati, Equation for the superfluid gap obtained by coarse graining the Bogoliubov-de Gennes equations throughout the BCS-BEC crossover, Phys. Rev. B **89**, 054511 (2014).

[14] S. Simonucci and G. C. Strinati, Non-local equation for the superconducting gap parameter, Phys. Rev. B **96**, 054502 (2017).

[15] O. T. Valls, M. Bryan, and I. Žutić, Superconducting proximity effects in metals with a repulsive pairing interaction, Phys. Rev. B **82**, 134534 (2010), and references therein.

[16] S. Kasahara, T. Yamashita, A. Shi, R. Kobayashi, Y. Shimoyama, T. Watashige, K. Ishida, T. Terashima, T. Wolf, F. Hardy, C. Meingast, H. v. Löhneysen, A. Levchenko, T. Shibauchi, and Y. Matsuda, Giant superconducting fluctuations in the compensated semimetal FeSe at the BCS-BEC crossover, Nat. Commun. **7**, 12843 (2016).

[17] N. I. Zheludev and Y. S. Kivshar, From metamaterials to metadevices, Nature Mater. **11**, 917 (2012), and references therein.

[18] Cf., e.g., J. D. Jackson, *Classical Electrodynamics* (Wiley, New York, 1999), Sec. 1.6.

[19] Alternatively, one could maintain the procedure of Appendix B in Ref. [14] also in the present 1D case whereby the gap parameter is neither even nor odd across the interface by extracting the even and odd components of the coupling and gap profiles by a suitable projection.

[20] In the present approach, the critical temperature T_c and the temperature-dependent gap parameter Δ deep in the (left or right) bulk regions are determined at the mean-field level for given coupling $(k_F a_F)^{-1}$ (cf. Ref. [2]).

[21] Cf., e.g., M. Le Bellac, *Quantum and Statistical Field Theory* (Clarendon, Oxford, 1995), Sec. 1.4.

[22] Similar conclusions were drawn in Ref. [12] [cf. Fig. 10 therein] where the size of an isolated vortex calculated in terms of the BdG equations was compared with the coherence length obtained for a homogeneous system by including pairing fluctuations beyond the mean field.

[23] F. Pistolesi and G. C. Strinati, Evolution from BCS superconductivity to Bose condensation: Role of the parameter $k_F\xi$, Phys. Rev. B **49**, 6356 (1994).

[24] To avoid spurious oscillations in the calculation of the Fourier transform (22), we follow Ref. [14] and interpret the kernel $K(|Q||x_0)$ in the sense of distributions by multiplying it with the Gaussian factor e^{-Q^2/τ^2}. In practice, the value of $\tau = 20k_F$ proves sufficient for our purposes.

[25] S. Simonucci, P. Pieri, and G. C. Strinati, Temperature dependence of a vortex in a superfluid Fermi gas, Phys. Rev. B **87**, 214507 (2013).

[26] H. L. Sueur, P. Joyez, H. Pothier, C. Urbina, and D. Esteve, Phase Controlled Superconducting Proximity Effect Probed by Tunneling Spectroscopy, Phys. Rev. Lett. **100**, 197002 (2008).

[27] W. Magnus, F. Oberhettinger, and R. P. Soni, *Formulas and Theorems for the Special Functions of Mathematical Physics* (Springer-Verlag, New York, 1966), Sec. 5.5.